


Cross-plane thermal transport in MoS₂Amey G. Gokhale¹, Dhvaneel Visaria¹, and Ankit Jain^{*}
Mechanical Engineering Department, IIT Bombay, Mumbai 400076, India (Received 30 June 2021; revised 6 August 2021; accepted 20 August 2021; published 1 September 2021)

We study the cross-plane thermal transport in MoS₂ using density functional theory by adequately accounting for the effect of widespread van der Waals (vdW) forces. We show that past studies report a large variation in the reported values of cross-plane thermal conductivity due to no or limited benchmarking of vdW functionals in computations and variations in sample sizes in experiments. In particular, we show that the validation of the considered vdW functionals based on the correct reproduction of harmonic properties (structural parameters, heat capacity) only is insufficient for the correct description of the thermal transport physics. Further, after having validated the suitability of different functionals, we find that the phonons contributing to cross-plane conductivity have an order of magnitude larger mean free path than that for the basal-plane thermal transport in MoS₂ at room temperature. The cross-plane transport is quasiballistic with a more than 80% contribution coming from phonons having mean free paths larger than 500 nm. Furthermore, we demonstrate that four-phonon scattering lowers the cross-plane thermal conductivity by more than 35% at room temperature and is required for a correct description of cross-plane thermal transport physics in layered materials.

DOI: [10.1103/PhysRevB.104.115403](https://doi.org/10.1103/PhysRevB.104.115403)**I. INTRODUCTION**

Due to their exceptional material properties compared to their bulk counterparts, two-dimensional (2D) materials have attracted immense attention for their potential technological applications in the field of nanoelectronics [1], optoelectronics [2,3], and flexible electronics [4]. A combination of such 2D materials can be stacked on top of each other to engineer a heterostructure with remarkable electronic and thermal properties [5]. The individual layers of these materials are held together by weak van der Waals (vdW) interactions and the resulting material properties are strongly dependent on the nature and strength of the underlying interlayer interactions. For instance, in the case of few-layer MoS₂, the electronic band gap and mobility evolves with the interlayer thickness [6,7], thereby allowing potential applications in electronics [8,9], photonics [10], and thermoelectrics [8,9]. It is imperative to understand the role of such interlayer interactions on the technologically relevant material properties. The thermal transport across layers (cross-plane) is one such property that plays a critical role in deciding the device performance [11].

The experimental studies on the understanding of cross-plane thermal transport of layered materials are limited in the literature and the measured cross-plane thermal conductivity varies over a wide range. At a temperature of 300 K in MoS₂, for example, Liu *et al.* [12] reported a cross-plane thermal conductivity in the range of 2–2.5 W/m K which is a factor of 2 lower than that measured by Jiang *et al.* [13] (~4.8 W/m K). Past studies showed that such large variations are due to fluctuations in measurement conditions and sample thicknesses, both of which are challenging to control in experiments [14].

Since experimental studies on the cross-plane thermal transport properties of layered materials are limited, computational tools [particularly based on density functional theory (DFT)] can be of great use to understand the cross-plane transport properties of layered materials. The DFT-based calculations allow for the precise control of material parameters and are instrumental in novel material discovery by predicting structural [15], mechanical [16,17], thermal [18,19] optical [20], electrical [21,22], and magnetic [23] properties of materials for applications such as catalytic reactions [24], thermal management [25], and energy storage [26]. The commonly employed DFT exchange-correlation (XC) functionals [such as the local density approximation (LDA), generalized gradient approximation (GGA), and meta-GGA], however, fail in capturing the effect of vdW interactions. The effect of vdW interactions is considered by either adding an empirical damped dispersion correction *a posteriori* (such as Grimme-D2 [27] and Grimme-D3 [28]) or by developing new, truly nonlocal exchange-correlation functional (such as vdW-DF [29] and vdW-DF2 [30]). Since the interlayer interactions are predominantly due to vdW forces, the choice of vdW functional can significantly alter the predicted cross-plane thermal properties.

For a particular case of MoS₂, a recent investigation by Sood *et al.* suggested quasiballistic thermal transport across layers at room temperature [31]. The authors used LDA-XC-based DFT calculations and found that phonons with mean free paths larger than 200 nm contribute 50% to the cross-plane transport. Past studies have, however, revealed that the LDA XC functional overbinds and incorrectly describes the interlayer binding energy for layered materials [32]. Gandhi *et al.* [33] considered Grimme-D3 correction to the GGA-PBE-XC (where PBE stands for Perdew-Burke-Ernzerhof) functional to account for the vdW forces and obtained a factor

^{*}a_jain@iitb.ac.in

of 2 lower thermal conductivity than that reported by Sood *et al.* [31]. On a similar line, Lindroth *et al.* explored the suitability of three different vdW functionals based only on structure parameters and obtained a cross-plane thermal conductivity of 5.2 W/m K for MoS₂ at 300 K [32]. Other past studies on the role of diverse approaches to account for vdW interactions for material property predictions are limited to simple properties such as the lattice constant and interlayer binding energy [34,35]. Thermal conductivity, being a complex material property dependent on both lattice harmonicity and anharmonicity, requires not only a correct reproduction of the structural properties but also other anharmonic properties (not captured by binding energy or lattice constant). Therefore, the validation of different vdW functionals for the prediction of cross-plane thermal conductivity of MoS₂ is indispensable.

In this paper, we thoroughly investigate the cross-plane thermal transport in MoS₂ by first validating the applicability of the vdW functionals for monolayer and bulk MoS₂. We include vdW interactions through (a) empirical corrections (Grimme-D2 [27] and Grimme-D3 [28]), and (b) nonlocal functionals [vdW-DF [29], vdW-DF2 [30], and the revised Vydrov–van Voorhis nonlocal correlation functional (rVV10) [36]]. We emphasize that our objective is to test the applicability of these available functionals (not the functional development) for thermal transport studies. The readers are referred to Refs. [27–30,36] for more details of these considered functionals.

II. COMPUTATIONAL DETAILS

We calculate the thermal conductivities of the monolayer and bulk materials by solving the Boltzmann transport equation (BTE) iteratively along with the Fourier law as [37,38]

$$\kappa_x = \sum_i c_{\text{ph},i} v_{x,i}^2 \tau_i. \quad (1)$$

The summation in Eq. (1) is over all the phonon modes in the Brillouin zone and c_{ph} , v_x , and τ are the phonon specific heat, group velocity (x component), and scattering lifetime, respectively. The details regarding c_{ph} , v_x , and τ calculations are available elsewhere in Refs [38–40].

The computation of phonon heat capacity, group velocity, and lifetime calculations requires harmonic and anharmonic force constants. We obtain these force constants from the finite difference of DFT forces. We employ the plane-wave-based electronic-structure calculation package QUANTUM ESPRESSO with PBE optimized norm-conserving Vanderbilt pseudopotentials. The atomic positions are relaxed using an electronic wave-vector grid of $6 \times 6 \times 1$ ($5 \times 5 \times 2$) for a monolayer (bulk) structure to ensure the residual forces on each atom are less than 10^{-5} Ry/Å. The plane-wave energy cutoff is set at 60 Ry in all calculations. The DFT forces are obtained on $8 \times 8 \times 1$ ($5 \times 5 \times 2$) repeated computational cells consisting of 192 (300) atoms where one or more atoms are displaced from their equilibrium positions by 0.05 Å (obtained after due convergence) for monolayer (bulk) MoS₂. Our converged value of 0.05 Å is consistent with Lindroth *et al.* [32] but is different than 0.01–0.03 Å which is typically employed in bulk materials. For example, openly available thermal conductivity calculators such as PHONO3PY [41] and SHENGBTE [42] default

this finite-displacement amplitude to 0.02–0.03 Å. With a displacement of 0.01 Å, the predicted thermal conductivity [using the relaxation time approximation (RTA) of the BTE] of monolayer MoS₂ is underpredicted by 59% at 300 K.

The harmonic and cubic interaction cutoffs are set to capture all interactions until the fifth and third in-plane nearest-neighbor shells. The translational invariance constraint in the calculation of force constants is enforced using the Lagrangian approach presented by Li *et al.* [43]. The phonon thermal conductivity is obtained by solving the BTE iteratively for a phonon wave-vector grid of $80 \times 80 \times 1$ ($30 \times 30 \times 12$) for monolayer (bulk) MoS₂. The iterative solution, as opposed to the commonly used RTA, does not treat normal three-phonon scattering processes as resistive and is critical for the correct description of thermal transport physics in 2D materials. The layer thickness is set at an interlayer separation of the corresponding bulk structure in the calculation of the thermal conductivity of monolayer MoS₂ from different functionals. The thermal conductivities are converged to within 15% for both monolayer and bulk MoS₂ with no-vdW corrections with an RTA solution of the BTE for these choices of simulation parameters at a temperature of 300 K.

III. RESULTS

A. Functional validation

We start by first validating the choice of vdW functionals for the prediction of lattice thermal conductivity. For this, we consider basal-plane thermal transport in monolayer and bulk MoS₂. Since the correct description of the structural properties is a prerequisite for a correct description of other material properties, we first compare basal- and cross-plane lattice parameters as obtained from different choices of vdW functionals against the experimentally reported values in Table I.

The intralayer bonding of atoms predominantly determines the basal-plane lattice constant of 2D materials. As atoms bond through the same strong covalent interactions in monolayer and bulk MoS₂, the obtained basal-plane lattice constants are the same for both structures. The lattice constant obtained using the no-vdW correction is higher than (albeit within 1%) the experimentally measured value. This underbinding of atoms from the PBE functional is a known shortcoming of GGA functionals and has been reported in the literature for other materials [48]. The lattice constants obtained with empirical dispersion correction schemes (Grimme-D2 and Grimme-D3) and the rVV10 nonlocal functional are within 1% of the experimental values. Other nonlocal functionals yield a higher deviation and the predicted lattice constant from the vdW-DF2 functional is 4% larger than the experimentally measured value. The incorrect prediction of the lattice constant, however, could still result in the correct description of thermal transport, as has been shown previously for silicon [49].

The overprediction of the lattice constant by the vdW-DF2 nonlocal functional is indicative of the weak interatomic bonding and is also reflected in the lower phonon frequencies compared to that from the no-vdW and empirically corrected Grimme-D2 functionals as is shown in Fig. 1. The phonon

TABLE I. Role of vdW functionals on the predicted thermal properties of monolayer and bulk MoS₂ for heat flow in the in-plane (\parallel) and out-of-plane (\perp) directions at a temperature of 300 K. The average group velocities and Grüneisen parameters are obtained from heat capacity weighted averaging of all modes. The reported thermal conductivities are for a sample size of 10 μm (1 μm for values reported in parentheses).

Functional	Lattice constant (\AA)			C_m (J/mol K)	Average group velocity (m/s)		Grüneisen parameter		Thermal conductivity (W/m K)		
	Monolayer	Bulk			Bulk		Monolayer	Bulk	Monolayer	Bulk	
		(\parallel)	(\perp)		Monolayer	(\parallel)				(\parallel)	(\perp)
Experimental		3.16 [44,45]	12.29 [44,45]	63.65 [46]					67–101 [47]	85–110 [12]	2–2.5 [12]
No-vdW	3.186	3.187	14.068	56.36	1818	1786	1.29	1.29	136 (95)	140 (101)	0 (0)
Grimme-D2	3.194	3.194	12.345	63.93	1832	1725	1.18	1.12	169 (125)	152 (121)	7 (5)
Grimme-D3	3.169	3.170	12.411	64.28	1831	1738	1.30	1.26	152 (109)	138 (111)	8 (4)
vdW-DF	3.235	3.240	13.047	59.54	1797	1733	1.33	1.30	125 (92)	109 (91)	1 (1)
vdW-DF2	3.286	3.291	12.802	59.55	1734	1650	1.38	1.35	109 (81)	93 (78)	4 (3)
rVV10	3.215	3.219	12.362	63.39	1787	1673	1.32	1.29	139 (98)	117 (97)	9 (5)

frequencies obtained from the no-vdW and empirically corrected functionals are in good agreement with the inelastic x-ray scattering measurements [50]. Contrarily, for the vdW-DF2 functional, the phonon spectrum is shifted to lower phonon frequencies. This softening of phonon dispersion is observed across the entire Brillouin zone for all phonon modes as is reflected in the phonon density of states plots in Fig. 1. Accordingly, the average phonon group velocities, obtained as

$$v_{g,\text{avg}} = \sqrt{\frac{\sum_i c_{\text{ph},i} v_{g,i}^2}{\sum_i c_{\text{ph},i}}}, \quad (2)$$

are also reduced by as much as 5% (8%) for monolayer (bulk) MoS₂ in the case of the vdW-DF2 functional compared to that from the no-vdW or empirically corrected functionals.

The cross-plane lattice constant has a profound effect on the phonon heat capacity of layered materials. The phonon heat capacity is the ability of a material to store energy in the form of atomic vibrations. Naturally, closely packed

materials result in a larger heat capacity compared to loosely packed layers. In the case of the no-vdW functional, layers are loosely packed in computations than in experiments and, as such, the calculated heat capacity is an underprediction of the experimental value by 11%. Similarly, for vdW-DF and vdW-DF2 nonlocal functionals, both of which overpredict the intralayer spacing, the heat capacities are an underprediction of the experimental measurements. The empirically corrected functionals and rVV10 nonlocal functional correctly capture the interlayer spacing and consequently result in a less than 1% deviation from the experimental measurement.

The analysis so far on the predictability of structural properties by different functionals suggests the suitability of Grimme-D2, Grimme-D3, and rVV10 functionals for harmonic phonon properties (vibration frequency, group velocity, and heat capacity). For purely harmonic solids, there is no scattering of heat carriers and the thermal conductivity is infinite. For real solids, the intrinsic thermal conductivity is limited by phonon-phonon scattering arising from a finite anharmonicity of the interatomic interaction potential. This anharmonicity is characterizable using the Grüneisen parameters [49]. The heat capacity weighted average Grüneisen parameter γ_{avg} , obtained as

$$\gamma_{\text{avg}} = \frac{\sum_i c_{\text{ph},i} |\gamma_i|}{\sum_i c_{\text{ph},i}}, \quad (3)$$

where γ_i are the mode-dependent Grüneisen parameters, is reported in Table I for all considered functionals at a temperature of 300 K.

Compared to harmonic properties, Grüneisen parameters are more involved and are difficult to measure in experiments. For the particular case of MoS₂, comprehensive data on the experimental measurement of the Grüneisen parameters are lacking in the available literature. In the absence of this experimental data, the accuracy of different functionals can be gauged by comparing the predicted Grüneisen parameter of monolayer MoS₂ with that from the no-vdW functional. The monolayer reference is justified due to the absence of vdW interactions and, consequently, the correct description of interatomic interactions by the no-vdW functional.

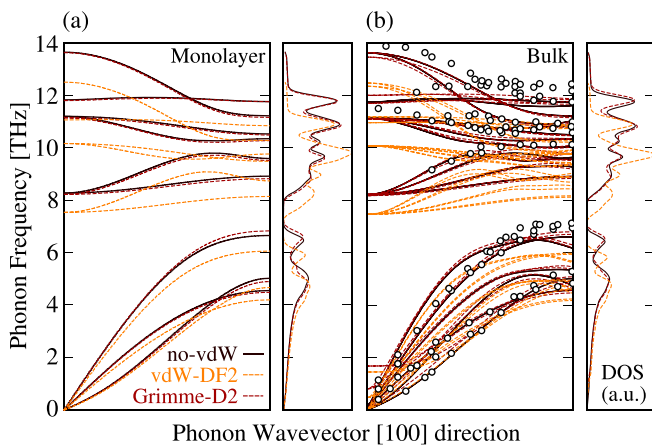


FIG. 1. Phonon dispersion and density of states (in arbitrary units) as obtained from no-vdW, Grimme-D2, and vdW-DF2 functionals for (a) monolayer and (b) bulk MoS₂. Experimentally measured frequencies [50] are also included for bulk MoS₂ in (b) using open symbols.

The average Grüneisen parameters obtained using Grimme-D3, vdW-DF, and rVV10 functionals are within 3% of the value predicted from the no-vdW functional. The values obtained from the Grimme-D2 and vdW-DF2 functionals are under- and overpredictions of the no-vdW value by 8% and 7%, respectively. It is worthwhile to note that both empirically corrected functionals have a similar functional form and differ only in the values of the dispersion coefficients [27,28]. However, for the Grimme-D3 functional with environment-dependent dispersion coefficients, the harmonic and anharmonic properties are correctly captured, but for the Grimme-D2 functional with only species-dependent coefficients, the anharmonic properties are erroneous. Further, it is interesting to note that while the Grimme-D2 functional is able to correctly predict the lattice constants and harmonic lattice properties, it severely underpredicts the lattice anharmonicity. Similarly, while the vdW-DF functional underbinds and hence overpredicts the lattice constant, the anharmonicity is correctly captured by the vdW-DF functional. This clearly shows that harmonic and anharmonic interactions are decoupled from each other and both are needed to be tested separately to check the suitability of a given functional for thermal conductivity prediction.

Now that we have tested the suitability of all the considered functionals for harmonic and anharmonic lattice properties, we next focus our attention on the thermal conductivity of MoS₂ at a temperature of 300 K. The basal-plane thermal conductivities of monolayer and bulk structures are compared with experimental measurements in Table I. As the experimental sample size is not explicitly mentioned in the literature studies, we report the predicted thermal conductivities by considering the boundary scattering lengths of 1 and 10 μm .

For the no-vdW functional, the predicted thermal conductivity is 95–136 W/m K for 1–10 μm wide monolayer samples, directly comparable with the experimental measurements. Due to the absence of vdW interactions in the monolayer arrangement of atoms, this computed thermal conductivity from the no-vdW functional can serve as a reference for the benchmarking of other functionals. With an exception of the Grimme-D2 and vdW-DF2 functionals, the predicted basal-plane thermal conductivities obtained from different functionals for a 10- μm monolayer sample are within 12% of the no-vdW value. For the Grimme-D2 and vdW-DF2 functionals, the predicted values are over- and underpredicted compared to the no-vdW monolayer case by 24% and 20% due to the under- and overprediction of crystal anharmonicity (and the harmonic properties for the vdW-DF2 functional). This indicates that even though vdW interactions are insignificant in monolayer materials, varying the computational treatment of vdW interactions can cause significant changes in the predicted basal-plane thermal conductivity.

For bulk MoS₂, the predicted basal-plane thermal conductivity from the considered functionals follows the same trend as that of monolayer samples, though the values are lower than the corresponding monolayer values due to additional damping of the basal-plane phonons from interlayer vdW interactions in the bulk configuration.

In contrast to the basal-plane thermal transport, the cross-plane thermal transport is primarily driven by weak interlayer vdW interactions. Accordingly, the cross-plane thermal

conductivities are (i) two orders of magnitude lower than the basal-plane values and (ii) have a profound dependence on the choice of vdW functional. The cross-plane thermal conductivity obtained from no-vdW is 0 due to the absence of any interlayer interactions. For the vdW-DF and vdW-DF2 functionals, both of which underbind and thus overpredict the experimentally observed interlayer separation, the obtained cross-plane thermal conductivities are 1–4 W/m K for a film thickness of 10 μm . The corresponding values predicted from empirical and rVV10 functionals are 7–9 W/m K compared to the experimentally measured value of 4.8 W/m K by Jiang *et al.* [13]. We believe that this overprediction is mainly due to a large sensitivity of cross-plane thermal transport on the film thickness, though atomic defects, stacking disorder, and higher-order phonon-phonon scattering could also be at play in reducing the thermal conductivity in experimental measurements. The effect of four-phonon scattering on the predicted thermal conductivity is discussed in Sec. III C.

The factor of 2 difference in the experimentally measured cross-plane thermal conductivities by Liu *et al.* [12] and Jiang *et al.* [13] is understandable from the strong thickness dependence of cross-plane transport. The calculations predict a factor of 2 reduction in thermal conductivity on decreasing the film thickness from 10 to 1 μm . Similarly, a large spread in the literature reported DFT-based cross-plane thermal conductivities is due to the use of a wide variety of vdW functionals without proper testing. In this study, we obtained values between 1 and 9 W/m K depending on the choice of functional. Our predicted cross-plane thermal conductivity from the validated Grimme-D3 and rVV10 functionals is 4–5 W/m K and is similar to a prediction by Lindroth *et al.* of 4 W/m K using the vdW-DF-CX functional [32] for a sample size of 1 μm .

B. Temperature- and mode-dependent thermal transport

We next focus our attention on the temperature- and mode-dependent transport properties of MoS₂ and report the temperature-dependent thermal conductivities as obtained from the Grimme-D3 functional in Fig. 2(a) and the corresponding thermal conductivity accumulation with phonon mean free paths in Fig. 2(b).

Overall, due to an increase in phonon-phonon scattering with increasing temperature, thermal conductivities decrease with temperature. The fall is sharper in the basal-plane direction and the thermal conductivity anisotropy ($\frac{k_x}{k_z}$) decreases from 29 at 100 K to 15 at 500 K [51]. Interestingly, even though cross-plane thermal conductivity is two orders of magnitude lower than the basal-plane value, the phonons contributing to cross-plane transport have an order of magnitude larger mean free path than that for the basal-plane transport [Fig. 2(b)], thereby suggesting a more profound effect of nanostructuring/sample size on cross-plane transport than on the basal-plane transport. Further, the range of contributing mean free paths is only over one order of magnitude for both basal- and cross-plane directions in MoS₂ as opposed to three to four orders of magnitude in silicon [49]. These steep accumulations suggest the possibility of tailoring the thermal transport anisotropy through nanostructuring. For instance, in the case of 0.5 μm samples, Fig. 2(b) suggests a cross-plane

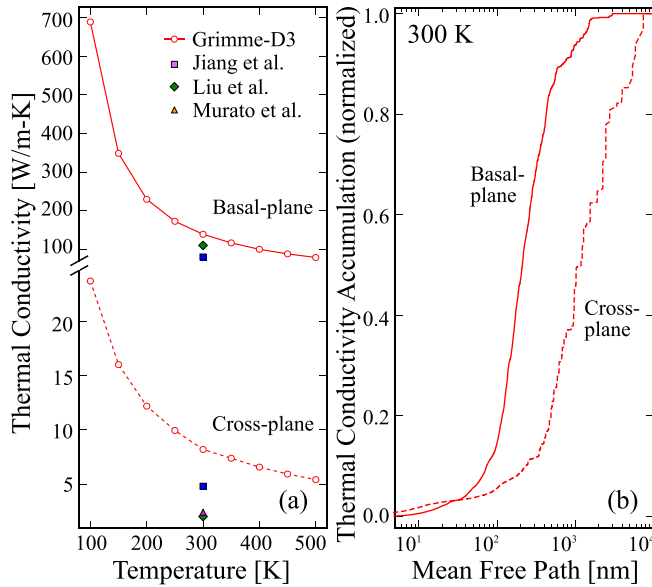


FIG. 2. (a) Temperature-dependent basal- and cross-plane thermal conductivities of bulk MoS₂ using the Grimme-D3 vdW functional, (b) Basal- and cross-plane thermal conductivity accumulation function with phonon mean free paths at 300 K. The thermal conductivities are obtained by considering phonon-boundary scattering corresponding to a characteristic length of 10 μm .

thermal conductivity reduction by 80% compared to only 20% for the basal plane, thus allowing for an increase in thermal conductivity anisotropy by a factor of 4.25.

C. Four-phonon scattering

Up to this point, all the reported thermal conductivities were obtained by considering only the lowest-order three-phonon scattering processes. While this lowest-order theory is sufficient in describing the thermal transport physics in moderate thermal conductivity solids, the scattering rates obtained by considering only the three-phonon processes are severely underpredicted for (a) high thermal conductivity materials such as graphene and boron arsenide (BAs) where three-phonon scattering is low and (b) strongly anharmonic solids such as Tl₃VSe₄ where atoms experience extremely anharmonic interatomic potentials [40,52]. The validity of the lowest-order theory is unclear for MoS₂, particularly for the cross-plane direction where thermal conductivity is an order of magnitude smaller than the basal-plane direction.

The effect of four-phonon scattering on the predicted thermal properties of MoS₂ is presented in Fig. 3. The reported results are obtained using the Grimme-D3 functional and correspond to thermal transport in a 10- μm -thick sample at 300 K. To cut down the computational cost of four-phonon scattering (which is otherwise 1000–10 000 \times computationally more expensive compared to the three-phonon scattering), the quartic force interactions are limited to nearest neighbors and the reported results are obtained using a phonon wave-vector grid of $16 \times 16 \times 8$ with the RTA solution of the BTE. The thermal conductivity obtained by considering only three-phonon scattering is 120 (8) W/m K using $16 \times 16 \times 8$ phonon wave-vector grid compared to 115 (8) W/m K using

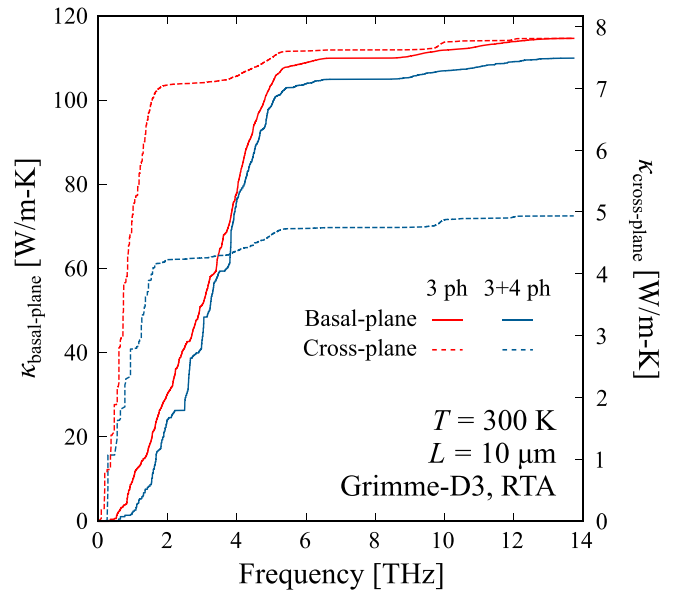


FIG. 3. The effect of four-phonon scattering on the basal- and cross-plane thermal transport properties of bulk MoS₂ at a temperature of 300 K. The results are obtained using the RTA solution of the BTE with a characteristic boundary scattering length of 10 μm .

a $30 \times 30 \times 12$ grid in the basal-plane (cross-plane) direction using the RTA solution of the BTE.

As can be seen from Fig. 3, the effect of four-phonon scattering is more pronounced for low-frequency phonons which have a relatively small three-phonon scattering phase space. Since these low-frequency phonons are a major contributor to the cross-plane transport, the cross-plane thermal conductivity reduces by more than 35% on the inclusion of four-phonon scattering while the decrease is less than 10% for the basal-plane transport. Nevertheless, long mean free path phonons remain the major carrier of heat in the cross-plane direction with a 61% (4%) contribution coming from phonons having a mean free path larger than 500 nm in the cross-plane (basal-plane) direction.

IV. CONCLUSIONS

In summary, we investigated the thermal transport in layered solids using the case of MoS₂ using a DFT-driven solution of the linearized BTE. This computational framework necessitates an appropriate validation of different vdW functionals. We compare the performance of empirically corrected (Grimme-D2 and Grimme-D3) and nonlocal (vdW-DF, vdW-DF2, and rVV10) functionals in predicting the harmonic (lattice constant, heat capacity) as well as anharmonic (basal- and cross-plane thermal transport) properties.

Interestingly, we find that the choice of vdW functionals is not only critical for the cross-plane thermal transport in bulk MoS₂ but also affects the basal-plane thermal transport in monolayer MoS₂ (with a variation up to 63% at 300 K). For cross-plane thermal transport across layers of bulk MoS₂, the values obtained from the vdW-DF and vdW-DF2 functionals are an underprediction of the Grimme-D3 and rVV10

values by up to an order of magnitude. After having validated the suitability of the Grimme-D3 and rVV10 functionals, on closely studying the cross-plane thermal transport in bulk MoS₂, we find that the cross-plane phonons have an order of magnitude larger mean free path than that for the basal-plane ones. Our calculations show that around 50% of heat is carried by phonons with a mean free path greater than 200 (165) nm and 1200 (425) nm in the basal- and cross-plane directions, respectively, for a sample size of 10(1) μm .

On investigating the role of higher-order four-phonon scattering processes, we find that the predicted basal-plane transport remains unaffected with the inclusion of four-phonon scattering. The cross-plane thermal conductivity, however, decreases by more than 35% at a temperature of

300 K in accordance with the soft bonding of atoms in the cross-plane direction.

The raw/processed data required to reproduce these findings are available upon reasonable request via email.

ACKNOWLEDGMENTS

The authors acknowledge the financial support from IRCC-IIT Bombay and National Supercomputing Mission, Government of India (Grant No. DST/NSM/R&D-HPC-Applications/2021/10). The calculations were carried out on SpaceTime-II supercomputing facility of IIT Bombay and PARAM Sanganak supercomputing facility of IIT Kanpur.

-
- [1] M. Dragoman, A. Dinescu, and D. Dragoman, *Phys. Status Solidi A* **216**, 1800724 (2019).
- [2] Q. H. Wang, K. Kalantar-Zadeh, A. Kis, J. N. Coleman, and M. S. Strano, *Nat. Nanotechnol.* **7**, 699 (2012).
- [3] K. F. Mak and J. Shan, *Nat. Photonics* **10**, 216 (2016).
- [4] S. J. Kim, K. Choi, B. Lee, Y. Kim, and B. H. Hong, *Annu. Rev. Mater. Res.* **45**, 63 (2015).
- [5] K. Novoselov, A. Mishchenko, A. Carvalho, and A. C. Neto, *Science* **353**, aac9439(2016).
- [6] K. F. Mak, C. Lee, J. Hone, J. Shan, and T. F. Heinz, *Phys. Rev. Lett.* **105**, 136805 (2010).
- [7] A. Kuc, N. Zibouche, and T. Heine, *Phys. Rev. B* **83**, 245213 (2011).
- [8] D. Wickramaratne, F. Zahid, and R. K. Lake, *J. Chem. Phys.* **140**, 124710 (2014).
- [9] S. Bhattacharyya, T. Pandey, and A. K. Singh, *Nanotechnology* **25**, 465701 (2014).
- [10] F. Yu, M. Hu, F. Kang, and R. Lv, *Prog. Nat. Sci.: Mater. Int.* **28**, 563 (2018).
- [11] J. C. Caylor, K. Coonley, J. Stuart, T. Colpitts, and R. Venkatasubramanian, *Appl. Phys. Lett.* **87**, 023105 (2005).
- [12] J. Liu, G.-M. Choi, and D. G. Cahill, *J. Appl. Phys.* **116**, 233107 (2014).
- [13] P. Jiang, X. Qian, X. Gu, and R. Yang, *Adv. Mater.* **29**, 1701068 (2017).
- [14] Q. Fu, J. Yang, Y. Chen, D. Li, and D. Xu, *Appl. Phys. Lett.* **106**, 031905 (2015).
- [15] Z. Wu, X. Hao, X. Liu, and J. Meng, *Phys. Rev. B* **75**, 054115 (2007).
- [16] M. Faghinasiri, M. Izadifard, and M. E. Ghazi, *J. Phys. Chem. C* **121**, 27059 (2017).
- [17] Z. Ding, S. Zhou, and Y. Zhao, *Phys. Rev. B* **70**, 184117 (2004).
- [18] A. Jain and A. J. H. McGaughey, *Phys. Rev. B* **93**, 081206(R) (2016).
- [19] A. Jain and A. J. McGaughey, *Sci. Rep.* **5**, 8501 (2015).
- [20] S. H. Brewer and S. Franzen, *Chem. Phys.* **300**, 285 (2004).
- [21] L.-D. Zhao, G. Tan, S. Hao, J. He, Y. Pei, H. Chi, H. Wang, S. Gong, H. Xu, V. P. Dravid *et al.*, *Science* **351**, 141 (2016).
- [22] Y. Wang, T. Gould, J. F. Dobson, H. Zhang, H. Yang, X. Yao, and H. Zhao, *Phys. Chem. Chem. Phys.* **16**, 1424 (2014).
- [23] L.-H. Ye, A. J. Freeman, and B. Delley, *Phys. Rev. B* **73**, 033203 (2006).
- [24] J. K. Nørskov, F. Abild-Pedersen, F. Studt, and T. Bligaard, *Proc. Natl. Acad. Sci. USA* **108**, 937 (2011).
- [25] M.-J. Lee, J.-H. Ahn, J. H. Sung, H. Heo, S. G. Jeon, W. Lee, J. Y. Song, K.-H. Hong, B. Choi, S.-H. Lee *et al.*, *Nat. Commun.* **7**, 12011 (2016).
- [26] X. Wu, F. Kang, W. Duan, and J. Li, *Prog. Nat. Sci.: Mater. Int.* **29**, 247 (2019).
- [27] S. Grimme, *J. Comput. Chem.* **27**, 1787 (2006).
- [28] S. Grimme, J. Antony, S. Ehrlich, and H. Krieg, *J. Chem. Phys.* **132**, 154104 (2010).
- [29] M. Dion, H. Rydberg, E. Schröder, D. C. Langreth, and B. I. Lundqvist, *Phys. Rev. Lett.* **92**, 246401 (2004).
- [30] K. Lee, É. D. Murray, L. Kong, B. I. Lundqvist, and D. C. Langreth, *Phys. Rev. B* **82**, 081101(R) (2010).
- [31] A. Sood, F. Xiong, S. Chen, R. Cheaito, F. Lian, M. Asheghi, Y. Cui, D. Donadio, K. E. Goodson, and E. Pop, *Nano Lett.* **19**, 2434 (2019).
- [32] D. O. Lindroth and P. Erhart, *Phys. Rev. B* **94**, 115205 (2016).
- [33] A. N. Gandhi and U. Schwingenschlögl, *Europhys. Lett.* **113**, 36002 (2016).
- [34] I. V. Lebedeva, A. V. Lebedev, A. M. Popov, and A. A. Knizhnik, *Comput. Mater. Sci.* **128**, 45 (2017).
- [35] S. A. Tawfik, T. Gould, C. Stampfl, and M. J. Ford, *Phys. Rev. Materials* **2**, 034005 (2018).
- [36] O. A. Vydrov and T. Van Voorhis, *J. Chem. Phys.* **133**, 244103 (2010).
- [37] J. M. Ziman, *Electrons and Phonons* (Oxford University Press/Clarendon, Oxford, UK, 1960).
- [38] J. A. Reissland, *The Physics of Phonons* (Wiley, New York, 1973).
- [39] A. J. McGaughey, A. Jain, H.-Y. Kim, and B. Fu, *J. Appl. Phys.* **125**, 011101 (2019).
- [40] A. Jain, *Phys. Rev. B* **102**, 201201(R) (2020).
- [41] A. Togo, L. Chaput, and I. Tanaka, *Phys. Rev. B* **91**, 094306 (2015).
- [42] W. Li, J. Carrete, N. A. Katcho, and N. Mingo, *Comput. Phys. Commun.* **185**, 1747 (2014).
- [43] W. Li, L. Lindsay, D. A. Broido, D. A. Stewart, and N. Mingo, *Phys. Rev. B* **86**, 174307 (2012).
- [44] T. Wieting and J. Verble, *Phys. Rev. B* **3**, 4286 (1971).
- [45] T. Böker, R. Severin, A. Müller, C. Janowitz, R. Manzke, D. Voß, P. Krüger, A. Mazur, and J. Pollmann, *Phys. Rev. B* **64**, 235305 (2001).

- [46] L. Volovik, V. Fesenko, A. Bolgar, S. Drozdova, L. Klochkov, and V. Primachenko, *Sov. Powder Metall. Met. Ceram.* **17**, 697 (1978).
- [47] X. Zhang, D. Sun, Y. Li, G.-H. Lee, X. Cui, D. Chenet, Y. You, T. F. Heinz, and J. C. Hone, *ACS Appl. Mater. Interfaces* **7**, 25923 (2015).
- [48] J. Harl and G. Kresse, *Phys. Rev. Lett.* **103**, 056401 (2009).
- [49] A. Jain and A. J. McGaughey, *Comput. Mater. Sci.* **110**, 115 (2015).
- [50] H. Tornatzky, R. Gillen, H. Uchiyama, and J. Maultzsch, *Phys. Rev. B* **99**, 144309 (2019).
- [51] H. P. Veeravenkata and A. Jain, *Carbon* **183**, 893 (2021).
- [52] N. K. Ravichandran and D. Broido, *Phys. Rev. X* **10**, 021063 (2020).